ATLAS NOTE

ATLAS-CONF-2012-011

March 2, 2012

Search for charged Higgs bosons decaying via $H^{\pm} \to \tau\nu$ in $t\bar{t}$ events using 4.6 fb^{-1} of pp collision data at $\sqrt{s} = 7$ TeV with the ATLAS detector

The ATLAS Collaboration

Abstract

The results of a search for charged Higgs bosons are presented. The analysis is based on 4.6 fb^{-1} of proton-proton (pp) collision data at $\sqrt{s} = 7$ TeV collected by the ATLAS experiment at the Large Hadron Collider, using $t\bar{t}$ events with a τ lepton in the final state. The data are consistent with the expected background from Standard Model processes. Assuming that the branching fraction $\mathcal{B}(H^{\pm} \to \tau\nu)$ is 100%, this leads to upper limits on $\mathcal{B}(t \to bH^{+})$ between 5% and 1% for charged Higgs boson masses ($m_{H^{+}}$) ranging from 90 to 160 GeV, respectively. In the context of the m_h^{max} scenario of the MSSM, values of $\tan\beta$ larger than 13–26 are excluded for charged Higgs boson masses in the range 90 GeV $< m_{H^{+}} <$ 150 GeV.

1 Introduction

Charged Higgs bosons (H^+, H^-) are predicted by several non-minimal Higgs scenarios, such as models containing Higgs triplets and Two Higgs Doublet Models (2HDM) [1]. The observation of a charged Higgs boson[1] would clearly indicate new physics beyond the Standard Model (SM). In a type-II 2HDM, such as the Higgs sector of the Minimal Supersymmetric [2–10] extension of the Standard Model (MSSM) [11–15], the main H^+ production mode at the Large Hadron Collider (LHC) is through top quark decays $t \to bH^+$, for charged Higgs boson masses smaller than the top quark mass (m_{top}). The dominant source of top quarks at the LHC is through $t\bar{t}$ production. The cross section for H^+ production from single top quark events is much smaller and not considered here. For $\tan\beta > 3$, where $\tan\beta$ is the ratio of the vacuum expectation values of the two Higgs doublets, the charged Higgs bosons decay dominantly via $H^+ \to \tau\nu$ [16]. In this paper, $\mathcal{B}(H^+ \to \tau\nu) = 100\%$ is always assumed. Under this assumption, the combined LEP lower limit for the charged Higgs boson mass is about 90 GeV [17]. At the Tevatron, no evidence for charged Higgs boson production in $p\bar{p}$ collisions has been found. Hence, the Tevatron experiments placed upper limits on $\mathcal{B}(t \to bH^+)$ in the 15–20% range for $m_{\text{H}^+} < m_{\text{top}}$ [18, 19].

This paper describes a search for charged Higgs bosons with masses in the range 90–160 GeV, using $t\bar{t}$ events with a leptonically or hadronically decaying τ in the final state, i.e. with the topology shown in Fig. 1. The results are based on 4.6 fb^{-1} of data from pp collisions at $\sqrt{s} = 7$ TeV, collected in 2011 with the ATLAS experiment [20] at the LHC. Three final states, which are expected to yield the highest sensitivity, are analysed:

- lepton+jets: $t\bar{t} \to b\bar{b}WH^+ \to b\bar{b}(q\bar{q}')(\tau_{\text{lep}}\nu)$, i.e. W decays hadronically and τ decays into an electron or a muon, with two neutrinos (generically referred to as "leptonic decays");
- τ+lepton: $t\bar{t} \to b\bar{b}WH^+ \to b\bar{b}(l\nu)(\tau_{\text{had}}\nu)$, i.e. W decays leptonically (with $l = e, \mu$) and τ decays hadronically;
- τ+jets: $t\bar{t} \to b\bar{b}WH^+ \to b\bar{b}(q\bar{q}')(\tau_{\text{had}}\nu)$, i.e. both W and τ decay hadronically.

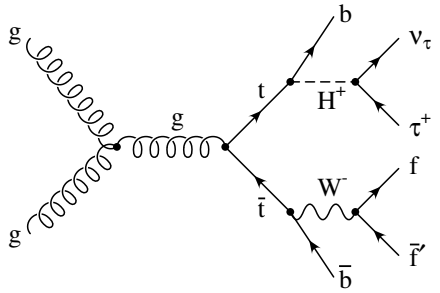

Figure 1: Example of a leading-order Feynman diagram for the production of $t\bar{t}$ events arising from gluon fusion, where one top quark decays to a charged Higgs boson, followed by $H^+ \to \tau\nu$.

[1] In the following, charged Higgs bosons are denoted H^+, with the charge-conjugate H^- always implied. Hence, if not otherwise specified, τ stands for a positively charged τ lepton.

2 Data and simulated events

The ATLAS detector consists of an inner tracking detector with coverage in pseudorapidity[2] up to $|\eta| = 2.5$, surrounded by a thin 2 T superconducting solenoid, a calorimeter system extending up to $|\eta| = 4.9$ for the detection of electrons, photons and hadronic jets, and a large muon spectrometer that measures the deflection of muon tracks in the field of three superconducting toroid magnets. Only data taken with all ATLAS sub-systems operational are used. Together with the requirement of having pp collisions at 7 TeV in stable beam conditions, this results in an integrated luminosity of 4.6 fb^{-1} for the 2011 data-taking period. The integrated luminosity has an uncertainty of 3.9% measured as described in Refs. [21, 22] and based on the whole 2011 data set.

The background processes that enter the search for a charged Higgs boson decaying via $H^+ \to \tau\nu$ in $t\bar{t}$ events include the SM pair production of top quarks $t\bar{t} \to b\bar{b}W^+W^-$, as well as the production of single top quark, W+jets, Z/γ^*+jets, diboson and multi-jet events. In order to give a realistic picture of the impact of the multi-jet background, data-driven methods are applied. Backgrounds with electrons or jets misidentified as hadronically decaying τ leptons are also estimated by using data-driven methods. The modeling of $t\bar{t}$ and single top quark events is performed with MC@NLO [23], except for the t-channel single top quark production where AcerMC [24] is used. The top quark mass is set to 172.5 GeV and the parton density function is CT10 [25]. For events generated with MC@NLO, the parton shower, hadronisation and underlying event are added using HERWIG [26] and JIMMY [27]. PYTHIA [28] is instead used for events generated with AcerMC. Inclusive cross sections are normalised to approximate next-to-next-to-leading order (NNLO) predictions of 167 pb for $t\bar{t}$ production [29], and 64.6 pb, 4.6 pb and 15.7 pb for single top quark production in the t-channel, s-channel and for Wt production, respectively [30–32]. Overlaps between the Wt and $t\bar{t}$ final states are removed [33]. Single vector boson (W and Z/γ^*) production is simulated with ALPGEN [34] interfaced to HERWIG and JIMMY, using CTEQ6.1 [35] parton density functions. The additional partons produced in the matrix element part of the event generation can be light partons or heavy quarks. In the latter case, dedicated samples with matrix elements for the production of massive $b\bar{b}$ or $c\bar{c}$ pairs are used. Diboson events (WW, WZ and ZZ) are generated using HERWIG. The cross sections are normalised to NNLO predictions for W and Z/γ^* production [36,37] and to next-to-leading order (NLO) predictions for diboson production [38].

The SM background samples are summarised in Table 1. In addition, three types of signal samples are produced with PYTHIA for 90 GeV $< m_{H^+} <$ 160 GeV: $t\bar{t} \to b\bar{b}H^+W^-$, $t\bar{t} \to b\bar{b}H^-W^+$ and $t\bar{t} \to b\bar{b}H^+H^-$, where the charged Higgs bosons decay as $H^+ \to \tau\nu$. The cross section for each of these three processes depends only on the total $t\bar{t}$ production cross section and the branching fraction $\mathcal{B}(t \to bH^+)$. TAUOLA [39] is used for τ decays, and PHOTOS [40] is used for photon radiation from charged leptons.

The event generators are tuned in order to describe the ATLAS data. The parameter sets AUET2 [41] and AUET2B [42] are used for events for which hadronisation is simulated using HERWIG/JIMMY and PYTHIA, respectively. To take into account the presence of multiple interactions (around 9, on average) occurring in the same and neighbouring bunch crossings (referred to as pile-up), and thereby overlapping signals in the detector, simulated minimum bias events are added to the hard process in each generated event. Prior to the analysis, simulated events are reweighted in order to match the distribution of the average number of pile-up interactions in the data. All generated events are propagated through

[2] ATLAS uses a right-handed coordinate system with its origin at the nominal interaction point (IP) in the centre of the detector and the z-axis along the beam pipe. The x-axis points from the IP to the centre of the LHC ring, and the y-axis points upwards. Cylindrical coordinates (r, ϕ) are used in the transverse plane, ϕ being the azimuthal angle around the beam pipe. The pseudorapidity is defined in terms of the polar angle θ as $\eta = -\ln\tan(\theta/2)$.

Process	Generator	Cross section [pb]	
$t\bar{t}$ with at least one lepton $\ell = e, \mu, \tau$	MC@NLO [23]	91	[29]
Single top quark t-channel (with ℓ)	AcerMC [24]	21	[30]
Single top quark s-channel (with ℓ)	MC@NLO [23]	1.5	[31]
Single top quark Wt-channel (inclusive)	MC@NLO [23]	16	[32]
$W \to \ell\nu$ + jets	ALPGEN [34]	3.1×10^4	[36]
$Z/\gamma^* \to \ell\ell$ + jets, $m(\ell\ell) > 10$ GeV	ALPGEN [34]	1.5×10^4	[37]
WW	HERWIG [26]	17	[38]
ZZ	HERWIG [26]	1.3	[38]
WZ	HERWIG [26]	5.5	[38]

Table 1: Cross sections for the SM background processes and generators used to model them.

a detailed GEANT4 simulation [43, 44] of the ATLAS detector and are reconstructed with the same algorithms as the data.

3 Physics object reconstruction

3.1 Data quality

Following basic data quality checks, further event cleaning is performed by demanding that no jet is consistent with having originated from instrumental effects, such as large noise signals in one or several channels of the hadronic end-cap calorimeter, coherent noise in the electromagnetic calorimeter, or non-collision backgrounds. In addition, events are discarded if the primary vertex (i.e. the reconstructed vertex with the largest sum of track momenta) has fewer than five associated tracks.

3.2 Electrons

Electrons are reconstructed by matching clustered energy deposits in the electromagnetic calorimeter to tracks reconstructed in the inner detector. The electron candidates are required to meet quality requirements based on the expected shower shape [45], to have $E_{\mathrm{T}} > 20$ GeV and to be in the fiducial volume of the detector, $|\eta| < 2.47$ (the transition region between the barrel and end-cap calorimeters, $1.37 < |\eta| < 1.52$, is excluded). Additionally, E_{T} and η-dependent calorimeter (tracking) isolation requirements are imposed in a cone with a radius[3] $\Delta R = 0.2$ (0.3) around the electron position, excluding the electron object itself, with an efficiency of about 90% for true electrons.

3.3 Muons

Muon candidates are required to contain matching inner detector and muon spectrometer tracks [46], as well as to have $p_{\mathrm{T}} > 15$ GeV and $|\eta| < 2.5$. Only isolated muons are accepted by requiring that, in a cone of radius $\Delta R = 0.2$ (0.3) around the muon, the transverse energy deposited in the calorimeters (the transverse momentum of the inner detector tracks) amounts to less than 4 GeV (2.5 GeV). The energy and momentum of the muon are excluded from the cone when making these isolation requirements.

[3] $\Delta R = \sqrt{(\Delta\eta)^2 + (\Delta\phi)^2}$, where $\Delta\eta$ is the difference in pseudorapidity of the two objects in question, and $\Delta\phi$ is the difference between their azimuthal angles.

3.4 Jets

Jets are reconstructed using the anti-k_t algorithm [47, 48] with a size parameter value of $R = 0.4$. The jet finder uses three-dimensional, noise-suppressed clusters of calorimeter cells [49], reconstructed at the electromagnetic energy scale. Jets are calibrated to the hadronic energy scale with correction factors based on simulation [50, 51]. A method that allows for the identification and selection of jets originating from the hard-scatter interaction through the use of tracking and vertexing information is used [52]. This is referred to as the "Jet Vertex Fraction" (JVF). The JVF measures the probability that a jet originated from a particular vertex and is defined by combining the tracks and their primary vertices with the calorimeter jets. By convention, jets with no associated tracks are assigned a JVF value of -1. The jet selection based on this discriminant is shown to be insensitive to the contributions from simultaneous uncorrelated soft collisions (i.e. pile-up). A requirement of $|\mathrm{JVF}| > 0.75$ is placed on all jets during event selection, i.e. after object reconstruction and overlap removal (defined in Section 3.6). In order to identify the jets initiated by b quarks, an algorithm is used that combines impact-parameter information with the explicit determination of a secondary vertex [53]. A working point is chosen that corresponds to an average efficiency of about 70% for b jets with $p_{\mathrm{T}} > 20$ GeV in $t\bar{t}$ events and a light-quark jet rejection factor of about 130. Since the b-tagger relies on the inner tracking detectors, the acceptance region for jets is restricted to $|\eta| < 2.4$.

3.5 τ jets

In order to reconstruct hadronically decaying τ leptons [54], anti-k_t jets with one or three associated tracks reconstructed in the inner detector and depositing $E_{\mathrm{T}} > 10$ GeV in the calorimeter are considered as τ candidates. Dedicated algorithms are used to reject electrons and muons. Hadronic τ decays are identified using a likelihood criterion designed to discriminate against quark- and gluon-initiated jets by using the shower shape and tracking variables as inputs. A working point with an efficiency of about 30% for hadronically decaying τ leptons with $p_{\mathrm{T}} > 20$ GeV in $Z \to \tau\tau$ events is chosen, leading to a rejection factor of about 100–1000 for quark- and gluon-initiated jets. The rejection factor depends on the p_{T} and η of the candidate, and the number of associated tracks. The τ candidates are further required to have a visible transverse momentum of at least 20 GeV and to be within $|\eta| < 2.3$. The selected τ candidates are henceforth referred to as "τ jets".

3.6 Removal of geometric overlaps between objects

When candidates selected using the criteria above overlap geometrically, the following procedure is applied, in this order: muon candidates are rejected if they are found within $\Delta R < 0.4$ of any jet with $p_{\mathrm{T}} > 25$ GeV and $|\mathrm{JVF}| > 0.75$; a τ jet is rejected if found within $\Delta R < 0.2$ of a selected muon or electron; jets are removed if they are within $\Delta R < 0.2$ of a selected τ object or electron.

3.7 Missing transverse momentum

The magnitude of the missing transverse momentum $E_{\mathrm{T}}^{\mathrm{miss}}$ [55] is reconstructed from three-dimensional, noise-suppressed clusters in the calorimeter, calibrated at the electromagnetic energy scale, and from muons reconstructed in the muon spectrometer. Clusters of calorimeter cells belonging to jets with $p_{\mathrm{T}} > 20$ GeV are calibrated to the hadronic energy scale. Calorimeter cells not associated with any object are taken into account and calibrated at the electromagnetic energy scale. Muons reconstructed in the inner tracking detectors are used to recover muons in regions not covered by the spectrometer. To deal appropriately with the energy deposited by muons in the calorimeters, the contributions of muons to $E_{\mathrm{T}}^{\mathrm{miss}}$ are calculated differently for isolated and non-isolated muons.

4 Lepton+jets channel

This analysis relies on the detection of lepton+jets decays of $t\bar{t}$ events, where the charged lepton l (electron or muon) arises from $H^+ \to \tau_{\text{lep}}\nu$, while the jets arise from a hadronically decaying W boson, i.e. $t\bar{t} \to b\bar{b}WH^+ \to b\bar{b}(q\bar{q}')(\tau_{\text{lep}}\nu)$. The analysis uses two variables that discriminate between leptons produced in $\tau \to l\nu_l\nu_\tau$ and leptons coming *directly* from W boson decays (with a mass $m_W < m_{H^+}$). The first discriminating variable is the invariant mass m_{bl} of the b jet and the charged lepton l coming from the same top quark candidate, or more conveniently, $\cos\theta_l^*$ defined as:

$$\cos\theta_l^* = \frac{2m_{bl}^2}{m_{\text{top}}^2 - m_W^2} - 1 \simeq \frac{4\,p^b \cdot p^l}{m_{\text{top}}^2 - m_W^2} - 1. \tag{1}$$

Both m_b^2 and m_l^2 are neglected, hence $m_{bl}^2 \simeq 2\,p^b \cdot p^l$, where p^b and p^l are the four-momenta of the b jet and of the charged lepton l, respectively. The presence of a charged Higgs boson in a leptonic top quark decay reduces the invariant product $p^b \cdot p^l$, when compared to W-mediated top quark decays, leading to $\cos\theta_l^*$ values closer to -1.

The second discriminating variable is the transverse mass m_{T}^H [56], obtained by fulfilling the constraint $(p^{\text{miss}} + p^l + p^b)^2 = m_{\text{top}}^2$ on the leptonic side of lepton+jets $t\bar{t}$ events. More than one neutrino accounts for p^{miss} and its transverse component $\vec{p}_{\text{T}}{}^{\text{miss}}$. The transverse mass is defined as:

$$(m_{\text{T}}^H)^2 = \left(\sqrt{m_{\text{top}}^2 + (\vec{p}_{\text{T}}{}^l + \vec{p}_{\text{T}}{}^b + \vec{p}_{\text{T}}{}^{\text{miss}})^2} - p_{\text{T}}^b\right)^2 - \left(\vec{p}_{\text{T}}{}^l + \vec{p}_{\text{T}}{}^{\text{miss}}\right)^2. \tag{2}$$

By construction, m_{T}^H gives an event-by-event lower bound on the mass of the leptonically decaying charged (W or Higgs) boson produced in the top quark decay.

4.1 Event selection

The lepton+jets analysis uses events passing a single-lepton trigger with an E_{T} threshold of 20–22 GeV for electrons[4] and a p_{T} threshold of 18 GeV for muons. These thresholds are low enough to guarantee that electrons and muons chosen for the analysis are in the plateau region of the trigger-efficiency curve. In addition, to select a sample of lepton+jets events enriched in $t\bar{t}$ candidates, the following requirements are applied:

- exactly one lepton having $E_{\text{T}} > 25$ GeV (electron) or $p_{\text{T}} > 20$ GeV (muon) and matched to the corresponding trigger object, with neither a second lepton nor a τ jet in the event;
- at least four jets having $p_{\text{T}} > 20$ GeV, $|\text{JVF}| > 0.75$ and $|\eta| < 2.4$, with exactly two of them being b-tagged;
- in order to select events with large $E_{\text{T}}^{\text{miss}}$, while rejecting those in which the latter arises from poorly reconstructed leptons, i.e. with a small azimuthal angle $\phi_{l,\text{miss}}$ between the lepton and $E_{\text{T}}^{\text{miss}}$:

$$\begin{array}{ll} E_{\text{T}}^{\text{miss}} > 40\ \text{GeV} & \text{if } |\phi_{l,\text{miss}}| \geq \pi/6, \\ E_{\text{T}}^{\text{miss}} \times |\sin(\phi_{l,\text{miss}})| > 20\ \text{GeV} & \text{if } |\phi_{l,\text{miss}}| < \pi/6. \end{array}$$

[4]The electron trigger threshold was increased towards the end of data-taking in 2011.

Having selected a lepton+jets sample enriched in $t\bar{t}$ candidates, jets must be assigned correctly to the decay products of each W boson and top quark. In particular, the hadronic side of the event is identified by selecting the combination of one b-tagged jet (b) and two untagged jets (j) that minimises:

$$\chi^2 = \frac{(m_{jjb} - m_{\text{top}})^2}{\sigma_{\text{top}}^2} + \frac{(m_{jj} - m_W)^2}{\sigma_W^2}, \tag{3}$$

where $\sigma_{\text{top}} = 17$ GeV and $\sigma_W = 10$ GeV are the widths of the reconstructed top quark and W boson, as measured in simulated $t\bar{t}$ events. Using information about the correctly-identified combinations in the generated events, the jet assignment efficiency is found to be 72%. Events with $\chi^2 > 5$ are rejected in order to select well-reconstructed hadronic top quark candidates.

4.2 Data-driven estimation of backgrounds with misidentified leptons

While the ATLAS lepton identification gives a very pure sample of candidates, there is a non-negligible contribution from non-isolated leptons arising from the semileptonic decay of b or c hadrons, from the decay-in-flight of $\pi^{\pm}$ or K mesons and, in the case of misidentified electron objects, from the reconstruction of π^0 mesons, photon conversions or shower fluctuations. All leptons coming from such mechanisms are referred to as *misidentified* leptons, as opposed to truly isolated leptons (e.g. from the decay of W or Z bosons), which are referred to as *real* leptons. The data-driven estimation of the number of misidentified leptons passing the lepton selections of Sections 3.2 and 3.3 is based on exploiting differences in the lepton identification between real and misidentified electrons or muons. Two data samples are defined, which differ only in the lepton identification criteria. The *tight* sample contains mostly events with real leptons and uses the same lepton selection as in the analysis. The *loose* sample contains mostly events with misidentified leptons. This latter sample is obtained by loosening the isolation and identification requirements for the leptons (the tight sample is therefore, by construction, a subset of the loose sample).

Let N_r^L and N_m^L (N_r^T and N_m^T) be the number of events containing real and misidentified leptons, respectively, passing a loose (tight) selection. The numbers of events containing one loose or tight lepton are given by:

$$N^L = N_m^L + N_r^L, \tag{4}$$

$$N^T = N_m^T + N_r^T. \tag{5}$$

Defining p_r and p_m as:

$$p_r = \frac{N_r^T}{N_r^L} \quad \text{and} \quad p_m = \frac{N_m^T}{N_m^L}, \tag{6}$$

the number of misidentified leptons passing the tight selection N_m^T can then be written as:

$$N_m^T = \frac{p_m}{p_r - p_m}(p_r N^L - N^T). \tag{7}$$

The main ingredients of this data-driven method are thus the efficiencies p_r and p_m for a real or a misidentified lepton, respectively, to be detected as a tight lepton. The lepton identification efficiency p_r is measured using a tag-and-probe method on $Z \to ll$ data events with a dilepton invariant mass between 86 and 96 GeV, where one lepton is required to fulfill tight selection criteria. The rate at which the other lepton passes the same tight selection criteria defines p_r. On the other hand, a control sample with misidentified leptons is selected by considering events in the data with exactly one lepton passing the loose criteria. To select events dominated by multi-jet production, $E_{\text{T}}^{\text{miss}}$ is required to be between 5 and 20 GeV. Residual true leptons contribute at a level below 10% and are subtracted from this sample

using simulation. After this subtraction, the rate at which a loose lepton passes tight selection criteria defines the misidentification rate p_m. In the final parameterisation of p_r and p_m, dependencies on the pseudorapidity of the lepton, its distance ΔR to the nearest jet, the leading jet p_{T} and the data-taking period are taken into account.

4.3 Reconstruction of discriminating variables after the selection cuts

The $\cos\theta_l^*$ distribution measured in the data is shown in Fig. 2(a), superimposed on the predicted background, determined with a data-driven method for the multi-jet background and simulation for the other SM backgrounds. A control region enriched in $t\bar{t} \to b\bar{b}W^+W^-$ events is defined by requiring $-0.2 < \cos\theta_l^* < 1$. This sample is used to fit the product of the cross section σ_{bbWW}, the luminosity, the selection efficiency, the acceptance and the branching ratio $\mathcal{B}(t \to bH^+)$ simultaneously with the likelihood for the signal estimation (see Section 8). In turn, this ensures that the final results, and in particular the upper limit on $\mathcal{B}(t \to bH^+)$, are independent of the assumed theoretical production cross section for $t\bar{t}$. With $\mathcal{B}(t \to bH^+) = 5\%$, the signal contamination in the control region ranges from 1.3% for $m_{H^+} = 90$ GeV to 0.4% for $m_{H^+} = 160$ GeV. The signal region is defined by requiring $\cos\theta_l^* < -0.6$ and $m_{\mathrm{T}}^W < 60$ GeV, where:

$$m_{\mathrm{T}}^W = \sqrt{2p_{\mathrm{T}}^l E_{\mathrm{T}}^{\mathrm{miss}}(1 - \cos\phi_{l,\mathrm{miss}})}. \tag{8}$$

This is done in order to enhance the selection of decays of charged (W or Higgs) bosons via $\tau \to l\nu_l\nu_\tau$. For events in the signal region, m_{T}^H, shown in Fig. 2(b), is used as a discriminating variable to search for charged Higgs bosons. Table 2 lists the contributions to the signal region of the SM processes and of $t\bar{t}$ events with at least one decay $t \to bH^+$, assuming $m_{H^+} = 130$ GeV and $B \equiv \mathcal{B}(t \to bH^+) = 5\%$. When including signal in the prediction, the simulated $t\bar{t}$ contribution is scaled by $(1 - B)^2$. The data are consistent with the predicted SM background and no significant deformation of the m_{T}^H distribution is observed.

Sample	Event yield (lepton+jets)
$t\bar{t}$	$840 \pm 20 \pm 150$
Single top quark	$28 \pm 2 \,^{+8}_{-6}$
W+jets	$14 \pm 3 \,^{+6}_{-3}$
Z+jets	$2.1 \pm 0.7 \,^{+1.2}_{-0.4}$
Diboson	$0.5 \pm 0.1 \pm 0.2$
Misidentified leptons	$55 \pm 10 \pm 20$
$\sum$ SM	$940 \pm 22 \pm 150$
Data	933
$t \to bH^+$ (130 GeV)	$120 \pm 4 \pm 25$
Signal+background	$990 \pm 21 \pm 140$

Table 2: Number of expected events in the signal region of the lepton+jets final state, and comparison with 4.6 fb^{-1} of data. Electroweak and $t\bar{t}$ backgrounds are estimated from simulation. A cross section of 167 pb is assumed for the $t\bar{t}$ background. Misidentified leptons from multi-jet backgrounds are estimated using a data-driven method. The numbers shown in the last two rows, for a hypothetical H^+ signal with $m_{H^+} = 130$ GeV, correspond to $\mathcal{B}(t \to bH^+) = 5\%$. Both statistical and systematic uncertainties are shown, in this order.

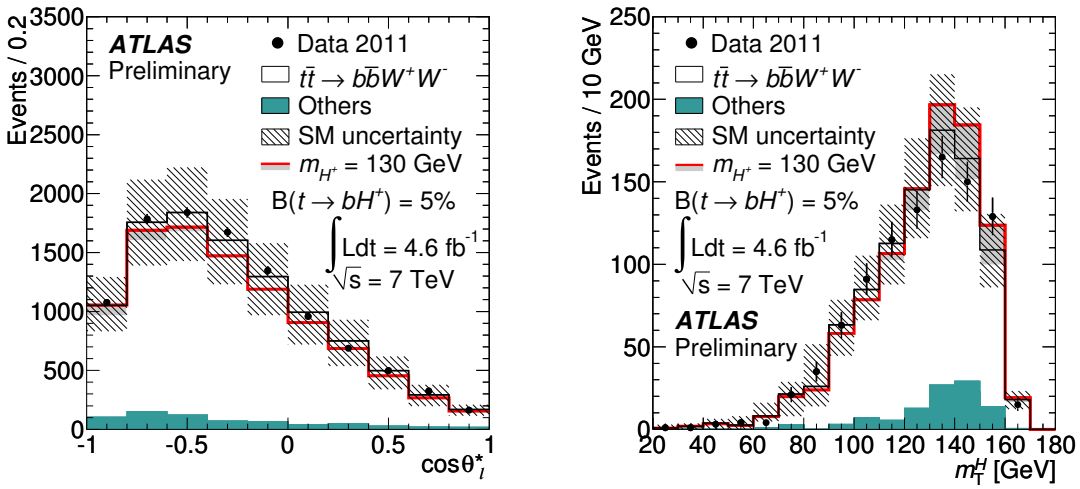

(a) (b)

Figure 2: Distribution of (a) $\cos\theta^*_l$ and (b) m_{T}^H, in the signal region ($\cos\theta^*_l < -0.6$, $m_{\mathrm{T}}^W < 60$ GeV) for the latter. The hatched area shows the total uncertainty for the SM backgrounds (see Section 7). "Others" refers to all SM backgrounds except $t\bar{t} \to b\bar{b}W^+W^-$. The red line shows the predicted contribution of signal+background in the presence of a 130 GeV charged Higgs boson, assuming $\mathcal{B}(t \to bH^+) = 5\%$ and $\mathcal{B}(H^+ \to \tau\nu) = 100\%$. The solid area below corresponds to the H^+ signal contribution.

5 τ+lepton channel

This analysis relies on the detection of τ+lepton decays of $t\bar{t}$ events, where the hadronically decaying τ arises from $H^+ \to \tau_{\mathrm{had}}\nu$, while the lepton (electron or muon) comes from the decay of the W boson, i.e. $t\bar{t} \to b\bar{b}WH^+ \to b\bar{b}(l\nu)(\tau_{\mathrm{had}}\nu)$. The background with misidentified leptons is estimated as in the lepton+jets analysis, and the other SM backgrounds are organised according to the true object associated with the detected τ jet.

5.1 Event selection

The τ+lepton analysis relies on the same single-lepton trigger signatures as the lepton+jets analysis presented in Section 4. In order to select τ+lepton events, the following requirements are made:

- exactly one lepton, having $E_{\mathrm{T}} > 25$ GeV (electron) or $p_{\mathrm{T}} > 20$ GeV (muon) and matched to the corresponding trigger object, and no other electron or muon;
- exactly one τ jet having $p_{\mathrm{T}} > 20$ GeV and an electric charge opposite to that of the lepton;
- at least two jets having $p_{\mathrm{T}} > 20$ GeV, |JVF| > 0.75 and $|\eta| < 2.4$, including at least one b-tagged jet;
- $\sum p_{\mathrm{T}} > 100$ GeV, where $\sum p_{\mathrm{T}}$ is the sum of the transverse momenta of all tracks associated with the primary vertex. Tracks entering the sum must pass quality cuts on the number of hits and have $p_{\mathrm{T}} > 1$ GeV.

$E_{\mathrm{T}}^{\mathrm{miss}}$ is used as the discriminating variable to distinguish between SM $t\bar{t}$ events and those where the top quark decays are mediated by a charged Higgs boson, in which case the neutrinos are likely to carry away more energy.

5.2 Data-driven estimation of backgrounds with misidentified leptons

The estimation of the backgrounds with misidentified leptons uses the data-driven method described in Section 4.2. To implement the method, the dependence of real and misidentification rates on the b-tagged jet multiplicity is taken into account, as well as the requirement for one τ jet (instead of a τ jet veto).

5.3 Backgrounds with electrons and jets misidentified as τ jets

The background with electrons misidentified as τ jets is estimated using a $Z \to ee$ control region in the data [54], where one electron is reconstructed as a τ jet. Misidentification probabilities derived from the data are applied to all simulated τ+lepton events. Studies using simulation show that this application is valid, as the misidentification probabilities for $Z \to ee$ and $t\bar{t}$ events are similar.

A data-driven method based on a control sample enriched in W+jets events is used to measure the probability for a jet to be misidentified as a hadronically decaying τ lepton. Like jets from the hard process in the dominant $t\bar{t}$ background, jets in the control sample originate predominantly from quarks instead of gluons. The measured probability is used to predict the yield of events due to jet$\to \tau$ misidentification from the most important SM backgrounds with intrinsic $E_{\mathrm{T}}^{\mathrm{miss}}$. The main difference between $t\bar{t}$ and W+jets events is the different fraction of b jets, which is smaller in W+jets events. However, the probability for a b jet to be misidentified as a τ jet is smaller than the corresponding probability for a light-quark jet, because the average track multiplicity is higher for b jets. Also, variables measuring the mass enter the τ reconstruction, providing further discrimination between b jets and τ jets. Differences in jet composition (e.g. the ratio of gluons to quarks) between $t\bar{t}$ and W+jets, assessed using simulation, are taken into account as systematic uncertainties. These also cover the dependence of the probability on whether a b jet or a light-quark jet is misidentified a τ jet.

Events in the control region are required to pass the same single-lepton trigger, data quality and lepton requirements as in the τ+lepton event selection. Additionally, a τ candidate and $E_{\mathrm{T}}^{\mathrm{miss}} > 40$ GeV are required, and events with b-tagged jets are vetoed. Events with a true τ contribute at a level below 0.5%. The τ candidates are required to have $p_{\mathrm{T}} > 20$ GeV, $|\eta| < 2.3$, and cannot be within $\Delta R = 0.2$ of any electron or muon; they are also not required to pass τ identification. The jet$\to \tau$ misidentification probability is defined as the number of objects passing the full τ identification divided by the number prior to requiring identification. This misidentification probability is measured as a function of both p_{T} and η. In addition, it is evaluated separately for τ candidates with 1 or 3 associated tracks.

In order to predict the background for the charged Higgs boson search, the measured jet$\to \tau$ misidentification probability is applied to simulated $t\bar{t}$, single top quark, W+jets, Z/γ^*+jets and diboson events, which are required to pass the full event selection except for the τ identification. For these events, τ candidates not overlapping with a true τ lepton or a true electron, but otherwise fulfilling the same requirements as in the denominator of the misidentification probability, are identified. Each of them is considered separately to be potentially misidentified as a τ jet. In order to avoid counting the same object twice, each jet that corresponds to a τ candidate is removed from the event, affecting the number of reconstructed jets and the number of b-tagged jets. If, after taking this into consideration, the event passes the τ+lepton selection, it is counted as a background event with a weight given by the misidentification probability corresponding to the p_{T} and η of the τ candidate. The predicted number of events from this data-driven method and from simulation is shown in Table 3. Small differences are observed between the predictions from the data-driven method and simulation, however they are smaller than previously reported in Ref. [54].

Sample	Data-driven method [events]	Simulation [events]
$t\bar{t}$	900 ± 15	877 ± 6
W+jets	150 ± 3	145 ± 9
Single top quark	81 ± 1	61 ± 2
Z/γ^*+jets	44 ± 1	69 ± 4
Diboson	6 ± 1	8 ± 1

Table 3: Application of the misidentification probability obtained from W+jets events in the data, for the τ+lepton channel. The predictions of the background contributions based on data-driven misidentification probabilities and on simulation are given, with statistical uncertainties only. In both cases, all top quarks are assumed to decay via $t \to bW$ (i.e. no charged Higgs boson signal is included).

5.4 $E_{\mathrm{T}}^{\mathrm{miss}}$ distribution after the selection cuts

Table 4 shows the expected number of background events for the SM-only hypothesis and the observation in the data. The total number of predicted events (signal+background) in the presence of a 130 GeV charged Higgs boson with $\mathcal{B}(t \to bH^+) = 5\%$ is also shown. The τ+lepton analysis relies on the theoretical $t\bar{t}$ production cross section $\sigma_{t\bar{t}} = 167^{+17}_{-18}$ pb [29] for the background estimation. In the presence of a charged Higgs boson in the top quark decays, with a branching fraction $B \equiv \mathcal{B}(t \to bH^+)$, the contributions of $t\bar{t} \to b\bar{b}W^+W^-$ events in the backgrounds with true or misidentified τ jets are scaled by $(1 - B)^2$. The background with correctly reconstructed τ jets is obtained with simulation. The data are found to be consistent with the expectation for the background-only hypothesis. The $E_{\mathrm{T}}^{\mathrm{miss}}$ distributions for the $\tau + e$ and $\tau + \mu$ channels, after all selection cuts are applied, are shown in Fig. 3.

Sample	Event yield (τ+lepton)	
	$\tau + e$	$\tau + \mu$
True τ	430 ± 14 ± 59	570 ± 15 ± 75
Misidentified jet→ τ	510 ± 23 ± 86	660 ± 26 ± 110
Misidentified $e \to \tau$	33 ± 4 ± 5	34 ± 4 ± 6
Misidentified leptons	39 ± 10 ± 20	90 ± 10 ± 34
$\sum$ SM	1010 ± 30 ± 110	1360 ± 30 ± 140
Data	880	1219
$t \to bH^+$ (130 GeV)	220 ± 6 ± 29	310 ± 7 ± 39
Signal+background	1160 ± 30 ± 100	1570 ± 30 ± 130

Table 4: Number of expected events after all selection cuts in the τ+lepton channel and comparison with 4.6 fb^{-1} of data. The numbers in the last two rows, for a hypothetical H^+ signal with $m_{H^+} = 130$ GeV, correspond to $\mathcal{B}(t \to bH^+) = 5\%$. All other rows assume $\mathcal{B}(t \to bW) = 100\%$. Both statistical and systematic uncertainties are shown, in this order.

6 τ+jets channel

The analysis presented here relies on the detection of τ+jets decays of $t\bar{t}$ events, where the hadronically decaying τ arises from $H^+ \to \tau_{\mathrm{had}}\nu$, while the jets come from a hadronically decaying W boson, i.e. $t\bar{t} \to b\bar{b}WH^+ \to b\bar{b}(q\bar{q}')(\tau_{\mathrm{had}}\nu)$.

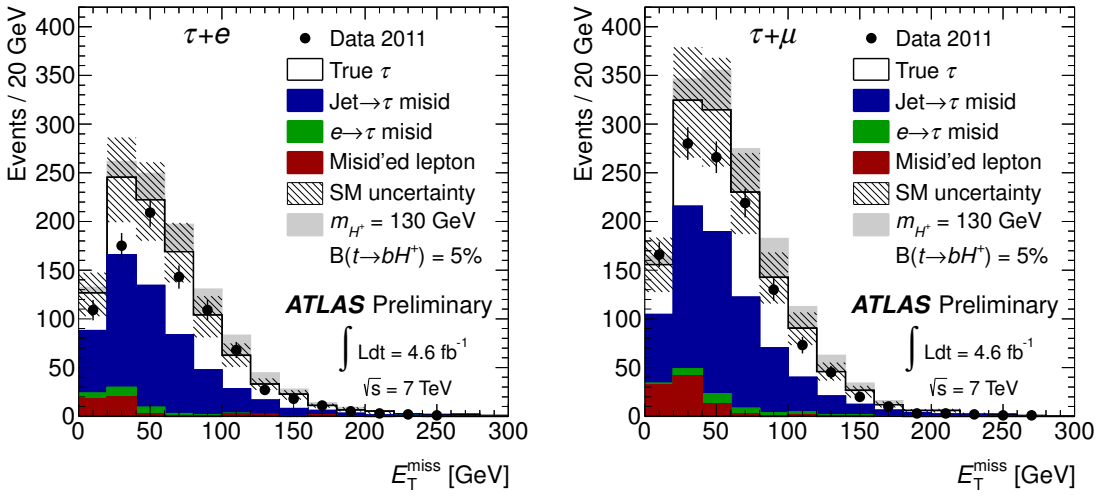

(a) (b)

Figure 3: $E_{\mathrm{T}}^{\mathrm{miss}}$ distribution after all selection cuts in the τ+lepton channel, for (a) τ+electron and (b) τ+muon final states. The hatched area shows the total uncertainty for the SM backgrounds (see Section 7). The stacked histogram shows the predicted contribution of signal+background in the presence of a 130 GeV charged Higgs boson with $\mathcal{B}(t \to bH^+) = 5\%$ and $\mathcal{B}(H^+ \to \tau\nu) = 100\%$. The contributions of $t\bar{t} \to b\bar{b}W^+W^-$ events in the backgrounds with true or misidentified τ jets are scaled down accordingly (see text).

6.1 Event selection

The τ+jets analysis uses events passing a $\tau + E_{\mathrm{T}}^{\mathrm{miss}}$ trigger with a threshold of 29 GeV on the τ object and 35 GeV on calorimeter-based $E_{\mathrm{T}}^{\mathrm{miss}}$. The following requirements are applied, in this order:

- at least 4 jets (excluding τ jets) having $p_{\mathrm{T}} > 20$ GeV, |JVF| > 0.75 and $|\eta| < 2.4$, of which at least one is b-tagged;
- exactly one τ jet with $p_{\mathrm{T}}^{\tau} > 40$ GeV, found within $|\eta| < 2.3$ and matched to a τ trigger object;
- neither a second τ jet with $p_{\mathrm{T}}^{\tau} > 20$ GeV, nor any electrons with $E_{\mathrm{T}} > 20$ GeV, nor any muons with $p_{\mathrm{T}} > 15$ GeV;
- $E_{\mathrm{T}}^{\mathrm{miss}} > 65$ GeV;
- to reject events in which a large reconstructed $E_{\mathrm{T}}^{\mathrm{miss}}$ is due to the limited resolution of the energy measurement, the $E_{\mathrm{T}}^{\mathrm{miss}}$ significance based on the $\sum p_{\mathrm{T}}$ definition of Section 5 must satisfy:

$$\frac{E_{\mathrm{T}}^{\mathrm{miss}}}{0.5 \cdot \sqrt{\sum p_{\mathrm{T}}}} > 13 \text{ GeV}^{1/2};$$

- a topology consistent with a top quark decay, by requiring the jjb candidate with the highest p_{T}^{jjb} to satisfy $m_{jjb} \in [120, 240]$ GeV.

For the selected events, the transverse mass m_{T} is defined as:

$$m_{\mathrm{T}} = \sqrt{2 p_{\mathrm{T}}^{\tau} E_{\mathrm{T}}^{\mathrm{miss}} (1 - \cos\phi_{\tau,\mathrm{miss}})}, \tag{9}$$

where $\phi_{\tau,\mathrm{miss}}$ is the azimuthal angle between the τ jet and the missing energy direction. This discriminating variable is related to the W boson mass in the $W \to \tau\nu$ background case and to the H^+ mass for the signal hypothesis.

6.2 Data-driven estimation of the multi-jet background

The multi-jet background is estimated by fitting its $E_{\mathrm{T}}^{\mathrm{miss}}$ shape (and the $E_{\mathrm{T}}^{\mathrm{miss}}$ shape of other backgrounds) to data. In order to study this shape in a data-driven way, a control region is defined where the τ identification and b-tagging requirements are modified, i.e. τ candidates must pass a loose τ identification but fail the tight τ identification used in the signal selection, and the event is required not to contain any b-tagged jet (hence, the requirement on m_{jjb} is also removed). Assuming that the shapes of the $E_{\mathrm{T}}^{\mathrm{miss}}$ and m_{T} distributions are the same in the control and signal regions, the $E_{\mathrm{T}}^{\mathrm{miss}}$ shape for the multi-jet background is measured in the control region, after subtracting the simulated background contributions from other processes. These other processes amount to less than 1% of the observed events in the control region. The $E_{\mathrm{T}}^{\mathrm{miss}}$ shapes obtained with the τ+jets selection of Section 6.1 or in the control region are compared early in the selection cut flow in Fig. 4(a). The differences between the two distributions are accounted for as systematic uncertainties. For the baseline selection, the $E_{\mathrm{T}}^{\mathrm{miss}}$ distribution measured in the data is then fit using two shapes: the multi-jet model and the sum of other processes (dominated by $t\bar{t}$ and W+jets), for which the shape and the relative normalisation are taken from simulation, as shown in Fig. 4(b). The ratio of multi-jet background events in the control and signal regions enters the likelihood function for the signal estimation (see Section 8) as a nuisance parameter while the shape of the multi-jet background is measured in the same region after additionally requiring $E_{\mathrm{T}}^{\mathrm{miss}} > 65$ GeV.

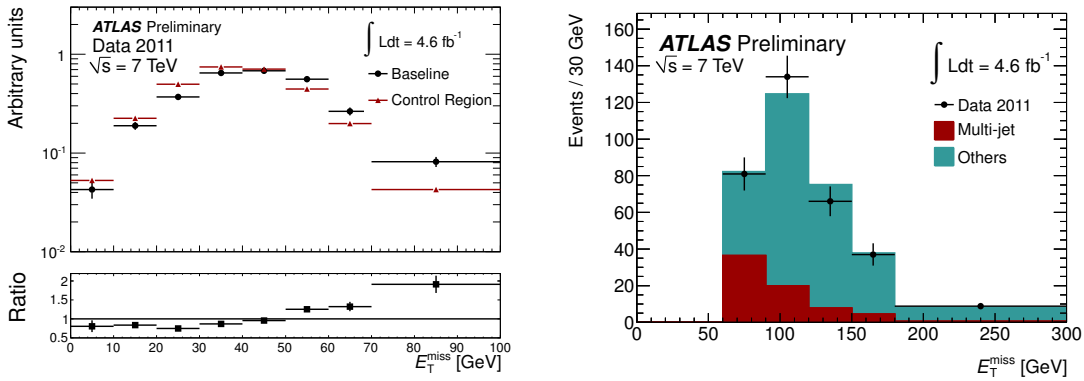

(a) (b)

Figure 4: (a) Shape of $E_{\mathrm{T}}^{\mathrm{miss}}$ in a control region of the data or using the baseline selection, after subtracting the expectation from $t\bar{t}$, W+jets, and single top quark processes estimated from simulation. The distributions are compared just before the $E_{\mathrm{T}}^{\mathrm{miss}}$ requirement in the baseline selection of Section 6.1, with the exception that, in the control region, the τ selection and the b-tagging requirements are modified, see text. (b) Fit of the $E_{\mathrm{T}}^{\mathrm{miss}}$ template to data, in the signal region. Only statistical uncertainties are shown.

6.3 Backgrounds with electrons and jets misidentified as τ jets

The methods described in Section 5.3 are used to estimate the probability for electrons or jets to be misidentified as τ jets. The estimated contribution to the background from the jet$\to \tau$ misidentification after the τ+jets selection is given in Table 5. Small differences are observed between the predictions from the data-driven method and simulation, however they are smaller than previously reported in Ref. [54].

Sample	Data-driven method [events]	Simulation [events]
$t\bar{t}$	33 ± 1	37 ± 1
W+jets	2.5 ± 0.1	3.9 ± 1.5
Single top quark	1.3 ± 0.1	2.0 ± 0.3

Table 5: Application of the misidentification probability obtained from a control region in the data enriched in W+jets events, for the τ+jets channel. The predictions of the background contributions based on data-driven misidentification probabilities and on simulation are given, with statistical uncertainties only. In both cases, all top quarks decay via $t \to bW$ (i.e. no charged Higgs boson signal is included).

6.4 Data-driven estimation of backgrounds with correctly reconstructed τ jets

An embedding method [57] is used to estimate the backgrounds that contain correctly reconstructed τ jets. The method consists of selecting a control sample of $t\bar{t}$-like μ+jets events and replacing the detector signature of the muon by a simulated hadronic τ decay. These new hybrid events are then used for the background prediction. In order to select this control sample from the data, the following event selection is applied:

- event triggered by a single-muon trigger (p_{T} threshold of 18 GeV);
- exactly one isolated muon with $p_{\mathrm{T}} > 25$ GeV, no isolated electron with $E_{\mathrm{T}} > 20$ GeV;
- at least four jets with $p_{\mathrm{T}} > 20$ GeV, with |JVF| > 0.75 and $|\eta| < 2.4$, at least one of which is b-tagged;
- $E_{\mathrm{T}}^{\mathrm{miss}} > 35$ GeV.

This selection is looser than the selection defined in Section 6.1 in order not to bias the control sample. The τ+jets event selection is then applied to the embedded events. The impurity from the background with muons produced in τ decays and non-isolated muons (dominantly $b\bar{b}$ and $c\bar{c}$ events) is about 10%. However, this contribution is greatly reduced as these events are much less likely to pass the τ+jets selection, in particular the p_{T}^{τ} requirement.

The shape of the m_{T} distribution for the backgrounds with true τ jets is taken from the distribution obtained with the embedded events. The normalisation is then derived from the number of embedded events:

$$N_{\tau} = N_{\mathrm{embedded}} \cdot \left(1 - c_{\tau\to\mu}\right) \frac{\epsilon^{\tau+E_{\mathrm{T}}^{\mathrm{miss}}-\mathrm{trigger}}}{\epsilon^{\mu-\mathrm{ID,trigger}}} \cdot \mathcal{B}(\tau \to \mathrm{hadrons} + \nu), \tag{10}$$

where N_{τ} is the estimated number of events with correctly reconstructed τ jets, N_{embedded} is the number of embedded events in the signal region, $c_{\tau\to\mu}$ is the fraction of events in which the selected muon is a decay product of a τ lepton (taken from simulation), $\epsilon^{\tau+E_{\mathrm{T}}^{\mathrm{miss}}-\mathrm{trigger}}$ is the $\tau + E_{\mathrm{T}}^{\mathrm{miss}}$ trigger efficiency (as a function of p_T^{τ} and $E_{\mathrm{T}}^{\mathrm{miss}}$, derived from data), $\epsilon^{\mu-\mathrm{ID,trigger}}$ is the muon trigger and identification efficiency (as a function of p_T and η, derived from data) and $\mathcal{B}(\tau \to \mathrm{hadrons} + \nu)$ is the branching ratio of the τ lepton decays involving hadrons. The m_{T} distribution for correctly reconstructed τ jets, as predicted by the embedding method, is shown in Fig. 5 and compared to simulation.

6.5 m_{T} distribution after the selection cuts

Table 6 shows the expected number of background events for the SM-only hypothesis and the observation in the data. The total number of predicted events (signal+background) in the presence of a 130 GeV

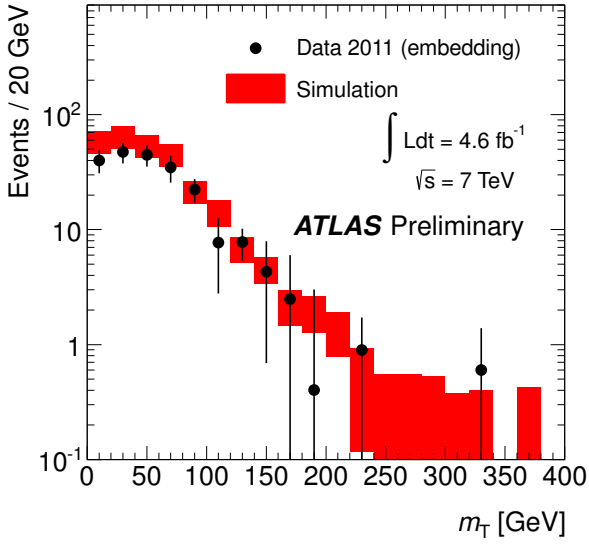

Figure 5: Comparison of the m_{T} distribution for correctly reconstructed τ jets, predicted by the embedding method and simulation. Combined statistical and systematic uncertainties (as described in Section 7) are shown.

charged Higgs boson with $\mathcal{B}(t \to bH^+) = 5\%$ is also shown. The number of events with a correctly reconstructed τ jet is derived from the number of embedded events and does not depend on the cross section of the $t\bar{t} \to b\bar{b}W^+W^-$ process. On the other hand, the τ+jets analysis relies on the theoretical inclusive $t\bar{t}$ production cross section $\sigma_{t\bar{t}} = 167^{+17}_{-18}$ pb [29] for the estimation of the background with electrons or jets misidentified as τ jets. In the presence of a charged Higgs boson in the top quark decays, with a branching fraction $B \equiv \mathcal{B}(t \to bH^+)$, the contributions of SM-like $t\bar{t} \to b\bar{b}W^+W^-$ events in these backgrounds are scaled by $(1 - B)^2$. The data are found to be consistent with the estimation of the SM background. The m_{T} distribution for the τ+jets channel, after all selection cuts are applied, is shown in Fig. 6.

Sample	Event yield (τ+jets)
True τ (embedding method)	210 ± 10 ± 44
Misidentified jet→ τ	36 ± 6 ± 10
Misidentified $e \to \tau$	3 ± 1 ± 1
Multi-jet processes	74 ± 3 ± 47
$\sum$ SM	330 ± 12 ± 65
Data	355
$t \to bH^+$ (130 GeV)	220 ± 6 ± 56
Signal+background	540 ± 13 ± 85

Table 6: Number of expected events after all selection cuts in the τ+jets channel and comparison with 4.6 fb^{-1} of data. The numbers in the last two rows, for a hypothetical H^+ signal with $m_{H^+} = 130$ GeV, correspond to $\mathcal{B}(t \to bH^+) = 5\%$. The rows for the backgrounds with misidentified objects assume $\mathcal{B}(t \to bW) = 100\%$. Both statistical and systematic uncertainties are shown, in this order.

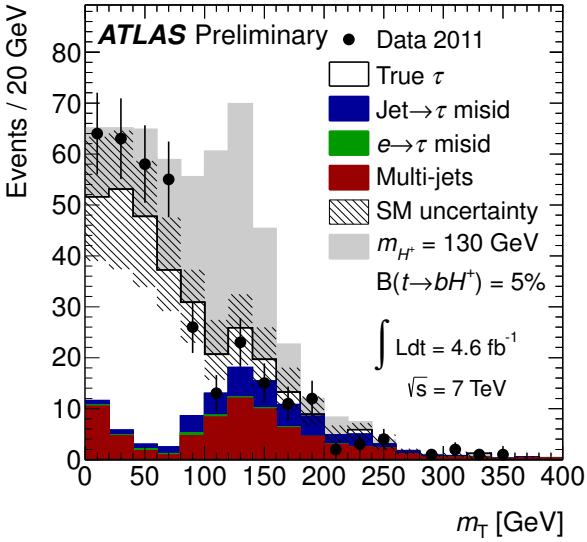

Figure 6: Distribution of m_{T} after all selection cuts in the τ+jets channel. The hatched area shows the total uncertainty for the SM backgrounds (see Section 7). The stacked histogram shows the predicted contribution of signal+background in the presence of a charged Higgs boson with $m_{H^+} = 130$ GeV, assuming $\mathcal{B}(t \to bH^+) = 5\%$ and $\mathcal{B}(H^+ \to \tau\nu) = 100\%$. The contributions of $t\bar{t} \to b\bar{b}W^+W^-$ events in the backgrounds with misidentified objects are scaled down accordingly (see text).

7 Systematic uncertainties

7.1 Systematic uncertainties arising from the detector simulation

Systematic uncertainties arising from the simulation of pile-up and object reconstruction are considered. The latter arise from the simulation of the trigger, the reconstruction and identification efficiencies, as well as the energy/momentum resolution and scale of the objects described in Section 3. To assess the impact of most sources of systematic uncertainty, the selection cuts for each analysis are re-applied after shifting a particular parameter by its ± 1 standard deviation uncertainty. The systematic uncertainties related to the electrons and muons are discussed in, respectively, Ref. [45] and Refs. [46, 58]. For the jets, see Ref. [51] and, in particular, Ref. [53] for the b-tagging calibration. The systematic uncertainties related to τ jets are discussed in Ref. [54]. Finally, for the reconstruction of $E_{\mathrm{T}}^{\mathrm{miss}}$, see Ref. [55]. All studies of systematic uncertainties have been updated with the full dataset collected in 2011. The dominant instrumental systematic uncertainties arise from the jet energy resolution (10–30%, depending on p_{T} and η), the jet energy scale (up to 14%, depending on p_{T} and η, to which a pile-up term of 2–7% and a b jet term of 2.5% are added in quadrature), as well as the b-tagging efficiency (5–17%, depending on p_{T} and η) and misidentification probability (12–21%, depending on p_{T} and η). In comparison, the systematic uncertainties arising from the reconstruction and identification of electrons and muons are small. All instrumental systematic uncertainties are also propagated to the reconstructed $E_{\mathrm{T}}^{\mathrm{miss}}$.

7.2 Systematic uncertainties arising from the generation of $t\bar{t}$ events

In order to estimate the systematic uncertainties arising from the $t\bar{t}$ generation and the parton shower model, the acceptance is computed for $t\bar{t}$ events produced with MC@NLO interfaced to HERWIG/JIMMY and POWHEG [59] interfaced to PYTHIA. For the signal samples, which are generated with PYTHIA

(i.e. without higher-order corrections), no alternative generator is available. Instead, the systematic uncertainty for the signal samples is set to the relative difference in acceptance between $t\bar{t}$ events generated with MC@NLO interfaced to HERWIG/JIMMY and AcerMC, which is also a leading-order generator, interfaced to PYTHIA. The systematic uncertainties arising from initial and final state radiation are computed using $t\bar{t}$ samples generated with AcerMC interfaced to PYTHIA, where initial and final state radiation parameters are set to a range of values not excluded by the experimental data [60]. The largest relative differences with respect to the reference sample after full event selections are used as systematic uncertainties. The systematic uncertainties arising from the modeling of the $t\bar{t}$ event generation and the parton shower, as well as initial and final state radiation, are summarised in Table 7 for each analysis.

Source of uncertainty	Normalisation uncertainty
lepton+jets:	
Generator and parton shower ($b\bar{b}WH^+$, signal region)	10%
Generator and parton shower ($b\bar{b}W^+W^-$, signal region)	8%
Generator and parton shower ($b\bar{b}WH^+$, control region)	7%
Generator and parton shower ($b\bar{b}W^+W^-$, control region)	6%
Initial and final state radiation (signal region)	8%
Initial and final state radiation (control region)	13%
τ+lepton:	
Generator and parton shower ($b\bar{b}WH^+$)	2%
Generator and parton shower ($b\bar{b}W^+W^-$)	5%
Initial and final state radiation	13%
τ+jets:	
Generator and parton shower ($b\bar{b}WH^+$)	5%
Generator and parton shower ($b\bar{b}W^+W^-$)	5%
Initial and final state radiation	19%

Table 7: Systematic uncertainties arising from the modeling of $t\bar{t} \to b\bar{b}W^+W^-$ and $t\bar{t} \to b\bar{b}WH^+$ events and the parton shower, as well as from initial and final state radiation.

7.3 Systematic uncertainties arising from data-driven background estimates

The systematic uncertainties arising from the data-driven methods used to estimate the various backgrounds are summarised in Table 8, for each of the three channels considered in the analysis.

For backgrounds with misidentified leptons, discussed in Sections 4.2 and 5.2, the main systematic uncertainties arise from the simulated samples used for subtracting true leptons in the determination of the misidentification probabilities. These are sensitive to the instrumental systematic uncertainties and from the sample dependence (misidentification probabilities are calculated in a control region dominated by gluon-initiated events, but later used in a data sample with a higher fraction of quark-initiated events).

The dominant systematic uncertainties in the estimation of the multi-jet background in the τ+jets channel, described in Section 6.2, are the statistical uncertainty of the fit due to the limited size of the data control sample and uncertainties due to potential differences of the $E_{\mathrm{T}}^{\mathrm{miss}}$ shape in the signal and control regions. The dominant systematic uncertainties in estimating the contribution of events with electrons misidentified as τ jets in Sections 5.3 and 6.3 arise from the subtraction of the multi-jet and electroweak backgrounds in the control region enriched with $Z \to ee$ events and from potential correlations in the

Source of uncertainty	Normalisation uncertainty	Shape uncertainty
lepton+jets: lepton misidentification		
Choice of control region	6%	-
Z mass window	4%	-
Jet energy scale	16%	-
Jet energy resolution	7%	-
Sample composition	31%	-
τ+lepton: jet$\rightarrow \tau$ misidentification		
Statistics in control region	2%	-
Jet composition	11%	-
Object-related systematics	23%	3%
τ+lepton: e$\rightarrow \tau$ misidentification		
Misidentification probability	20%	-
τ+lepton: lepton misidentification		
Choice of control region	4%	-
Z mass window	5%	-
Jet energy scale	14%	-
Jet energy resolution	4%	-
Sample composition	39%	-
τ+jets: true τ		
Embedding parameters	6%	3%
Muon isolation	7%	2%
Parameters in normalisation	16%	-
τ identification	5%	-
τ energy scale	6%	1%
τ+jets: jet$\rightarrow \tau$ misidentification		
Statistics in control region	2%	-
Jet composition	12%	-
Purity in control region	6%	1%
Object-related systematics	21%	2%
τ+jets: e$\rightarrow \tau$ misidentification		
Misidentification probability	22%	-
τ+jets: multi-jet estimate		
Fit-related uncertainties	32%	-
$E_{\mathrm{T}}^{\mathrm{miss}}$-shape in control region	16%	-

Table 8: Dominant systematic uncertainties on the data-driven estimates. The shape uncertainty is defined as the relative shift of the mean value of the final discriminant distribution. A "-" in the second column indicates negligible shape uncertainties.

selections of the tag and probe electrons. For the estimation of backgrounds with jets misidentified as hadronically decaying τ leptons, also discussed in Sections 5.3 and 6.3, the dominant systematic uncertainties on the misidentification probability are the statistical uncertainty due to the limited control sample size and uncertainties due to the difference of the jet composition (gluon or quark-initiated) in the control and signal regions, which is estimated using simulation. Other uncertainties come from the impurities arising from multi-jet background events and true hadronic τ leptons in the control sample. The systematic uncertainties affecting the estimation of the background from correctly reconstructed τ jets in the τ+jets channel, discussed in Section 6.4, consist of the potential bias introduced by the embedding method itself, uncertainties from the trigger efficiency measurement, uncertainties associated to simulated τ jets (τ energy scale and identification efficiency) and uncertainties on the normalisation, which are dominated by the statistical uncertainty of the selected control sample and the $\tau + E_{\mathrm{T}}^{\mathrm{miss}}$ trigger efficiency uncertainties.

8 Results

In order to test the compatibility of the data with background-only and signal+background hypotheses, a profile likelihood ratio [61] is used with m_{T}^{H} (lepton+jets), $E_{\mathrm{T}}^{\mathrm{miss}}$ (τ+lepton) and m_{T} (τ+jets) as the discriminating variables. The statistical analysis is based on a binned likelihood function for these distributions. The systematic uncertainties in shape and normalisation are incorporated via nuisance parameters, and the one-sided profile likelihood ratio, $\tilde{q}_{\mu}$, is used as a test statistic. No significant excess of events is observed in any of the investigated final states in 4.6 fb^{-1} of data. Exclusion limits are set on $\mathcal{B}(t \to bH^{+})$ and, in the context of the m_h^{max} scenario of the MSSM [62], on $\tan\beta$ for $m_{H^{+}}$ in the range 90–160 GeV, by rejecting the signal hypothesis at the 95% confidence level (CL) using the CL$_s$ procedure [63]. These limits are based on the asymptotic distribution of the test statistic [61]. The combined limit is derived from the product of the individual likelihoods, and systematic uncertainties are treated as correlated where appropriate. The exclusion limits for the individual channels, as well as the combined limit, are shown in Fig. 7 in terms of $\mathcal{B}(t \to bH^{+})$ with the assumption $\mathcal{B}(H^{+} \to \tau\nu) = 100\%$, and in Fig. 8 in terms of $\tan\beta$, in the context of the m_h^{max} scenario of the MSSM. No exclusion limit is shown for values of $m_{H^{+}}$ for which the limit on $\tan\beta$ is too high for reliable calculations of $\mathcal{B}(t \to bH^{+})$. The following relative theoretical uncertainties on $\mathcal{B}(t \to bH^{+})$ are considered [64,65]: 5% for one-loop electroweak corrections missing in the calculations, 2% for missing two-loop QCD corrections, and about 1% (depending on $\tan\beta$) for Δ_b-induced uncertainties (where Δ_b is a correction factor to the running bottom quark mass [66]). These uncertainties are added linearly, as recommended by the LHC Higgs cross section working group [65].

9 Conclusions

Charged Higgs bosons are searched for in the decay mode $t \to bH^{+}$, always followed by $H^{+} \to \tau\nu$, using $t\bar{t}$ events reconstructed in a total of 4.6 fb^{-1} of pp collision data at $\sqrt{s} = 7$ TeV, recorded in 2011 with the ATLAS experiment. Three final states are considered, which are characterised by the presence of a leptonic or hadronic τ decay, $E_{\mathrm{T}}^{\mathrm{miss}}$, b jets, and a leptonically or hadronically decaying W boson. Data-driven methods and simulation are employed to estimate the number of background events. The observed data are found to be in agreement with the SM predictions. Assuming $\mathcal{B}(H^{+} \to \tau\nu) = 100\%$, upper limits at the 95% confidence level have been set on the branching ratio $\mathcal{B}(t \to bH^{+})$ between 5% ($m_{H^{+}} = 90$ GeV) and 1% ($m_{H^{+}} = 160$ GeV). This result constitutes a significant improvement compared to existing limits provided by the Tevatron experiments [18, 19] over the whole investigated mass range, but in particular for $m_{H^{+}}$ close to the top quark mass. Interpreted in the context of the m_h^{max} scenario of the MSSM, values of $\tan\beta$ above 13–26 can be excluded in the mass range 90 GeV $< m_{H^{+}} <$ 150 GeV.

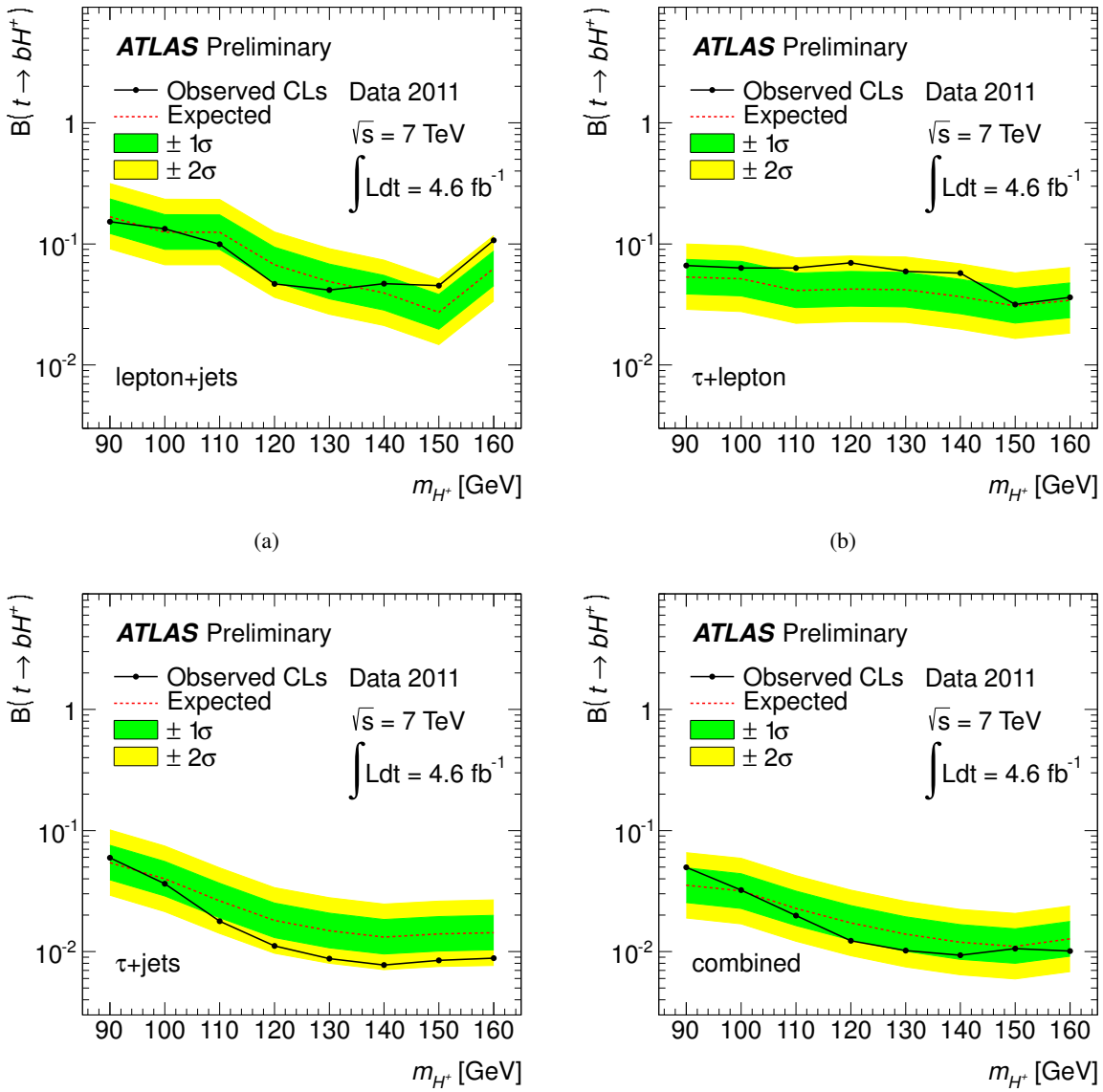

Figure 7: Expected and observed 95% CL exclusion limits on $\mathcal{B}(t \to H^+b)$ for charged Higgs boson production from top quark decays as a function of m_{H^+}, assuming $\mathcal{B}(H^+ \to \tau\nu) = 100\%$. Shown are the results for: (a) lepton+jets channel; (b) τ+lepton channel; (c) τ+jets channel; (d) combination.

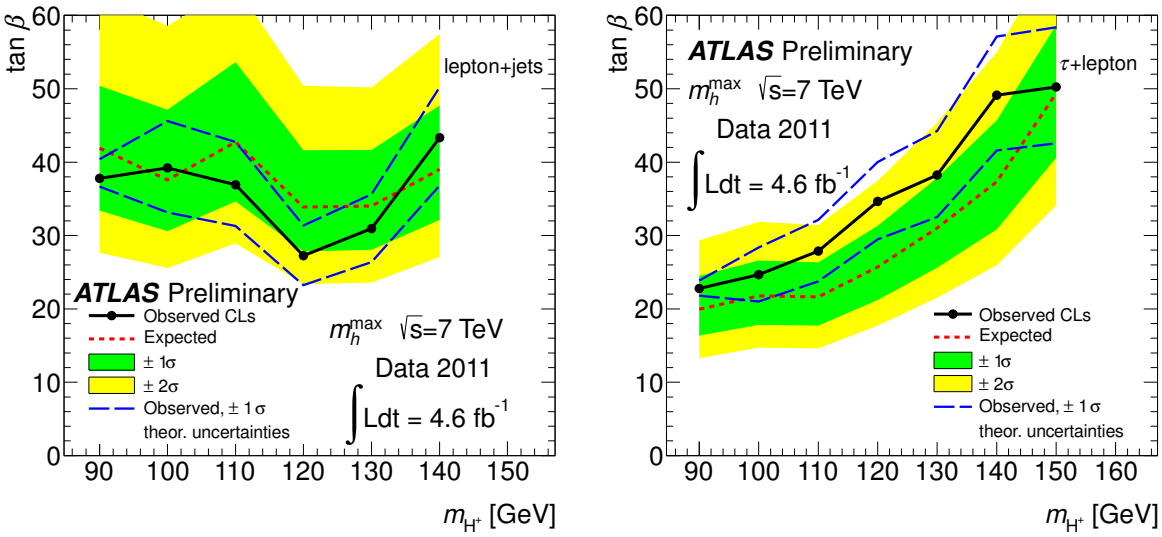

(a)

(b)

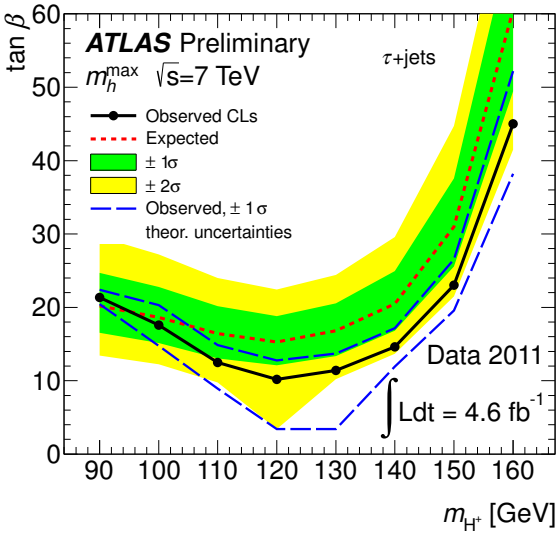

(c)

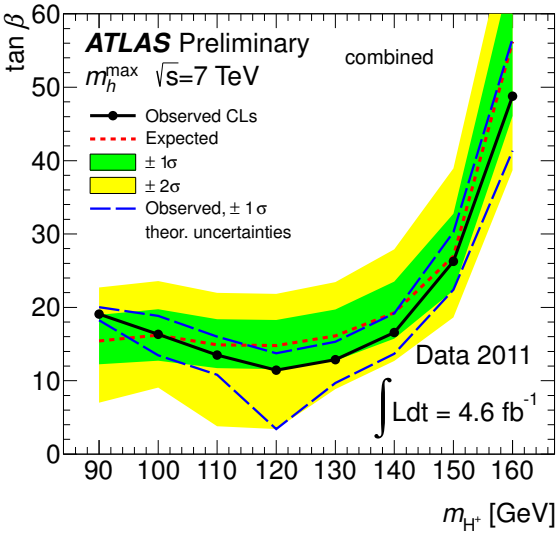

(d)

Figure 8: 95% CL exclusion limits on $\tan\beta$ as a function of m_{H^+}. Results are shown in the context of the MSSM scenario $m_h^{\max}$ for: (a) lepton+jets channel; (b) τ+lepton channel; (c) τ+jets channel; (d) combination. The blue dashed lines indicate the theoretical uncertainties on $\mathcal{B}(t \to bH^+)$ described in the text.

References

[1] T. Lee, *A Theory of Spontaneous T Violation*, *Phys. Rev.* **D8** (1973) 1226–1239.

[2] H. Miyazawa, *Baryon Number Changing Currents*, *Prog. Theor. Phys.* **36 (6)** (1966) 1266–1276.

[3] P. Ramond, *Dual Theory for Free Fermions*, *Phys. Rev.* **D3** (1971) 2415–2418.

[4] Y. A. Golfand and E. P. Likhtman, *Extension of the Algebra of Poincare Group Generators and Violation of p Invariance*, *JETP Lett.* **13** (1971) 323–326.

[5] A. Neveu and J. H. Schwarz, *Factorizable dual model of pions*, *Nucl. Phys.* **B31** (1971) 86–112.

[6] A. Neveu and J. H. Schwarz, *Quark Model of Dual Pions*, *Phys. Rev.* **D4** (1971) 1109–1111.

[7] J. Gervais and B. Sakita, *Field theory interpretation of supergauges in dual models*, *Nucl. Phys.* **B34** (1971) 632–639.

[8] D. V. Volkov and V. P. Akulov, *Is the Neutrino a Goldstone Particle?*, *Phys. Lett.* **B46** (1973) 109–110.

[9] J. Wess and B. Zumino, *A Lagrangian Model Invariant Under Supergauge Transformations*, *Phys. Lett.* **B49** (1974) 52.

[10] J. Wess and B. Zumino, *Supergauge Transformations in Four-Dimensions*, *Nucl. Phys.* **B70** (1974) 39–50.

[11] P. Fayet, *Supersymmetry and Weak, Electromagnetic and Strong Interactions*, *Phys. Lett.* **B64** (1976) 159.

[12] P. Fayet, *Spontaneously Broken Supersymmetric Theories of Weak, Electromagnetic and Strong Interactions*, *Phys. Lett.* **B69** (1977) 489.

[13] G. R. Farrar and P. Fayet, *Phenomenology of the Production, Decay, and Detection of New Hadronic States Associated with Supersymmetry*, *Phys. Lett.* **B76** (1978) 575–579.

[14] P. Fayet, *Relations Between the Masses of the Superpartners of Leptons and Quarks, the Goldstino Couplings and the Neutral Currents*, *Phys. Lett.* **B84** (1979) 416.

[15] S. Dimopoulos and H. Georgi, *Softly Broken Supersymmetry and SU(5)*, *Nucl. Phys.* **B193** (1981) 150.

[16] S. Dittmaier, C. Mariotti, G. Passarino, R. Tanaka, *et. al.*, *Handbook of LHC Higgs Cross Sections: 1. Inclusive Observables*, *CERN-2011-002* (2011) [arXiv:1101.0593].

[17] **LEP Higgs Working Group for Higgs boson searches, ALEPH, DELPHI, L3, OPAL** Collaboration, *Search for Charged Higgs bosons: Preliminary Combined Results Using LEP data Collected at Energies up to 209 GeV*, hep-ex/0107031.

[18] **CDF** Collaboration, T. Aaltonen *et. al.*, *Search for charged Higgs bosons in decays of top quarks in p-pbar collisions at* $\sqrt{s} = 1.96$ *TeV*, *Phys. Rev. Lett.* **103** (2009) 101803, [arXiv:0907.1269].

[19] **D0** Collaboration, V. M. Abazov *et. al.*, *Search for charged Higgs bosons in top quark decays*, *Phys. Lett.* **B682** (2009) 278–286, [arXiv:0908.1811].

[20] **ATLAS** Collaboration, *The ATLAS Experiment at the CERN Large Hadron Collider*, *JINST* **3** (2008) S08003.

[21] **ATLAS** Collaboration, *Luminosity Determination in pp Collisions at $\sqrt{s} = 7$ TeV using the ATLAS Detector in 2011*, *ATLAS-CONF-2011-116*. https://cdsweb.cern.ch/record/1376384.

[22] **ATLAS** Collaboration, *Luminosity Determination in pp Collisions at $\sqrt{s} = 7$ TeV Using the ATLAS Detector at the LHC*, *Eur. Phys. J. C* **71** (2011) 1630, [arXiv:1101.2185].

[23] S. Frixione and B. R. Webber, *Matching NLO QCD Computations and Parton Shower Simulations*, *JHEP* **0206** (2002) 029, [hep-ph/0204244].

[24] B. P. Kersevan and E. Richter-Was, *The Monte Carlo Event Generator AcerMC version 2.0 with Interfaces to PYTHIA 6.2 and HERWIG 6.5*, hep-ph/0405247.

[25] H.-L. Lai, M. Guzzi, J. Huston, Z. Li, P. M. Nadolsky, *et. al.*, *New parton distributions for collider physics*, *Phys. Rev.* **D82** (2010) 074024, [arXiv:1007.2241].

[26] G. Corcella, I. Knowles, G. Marchesini, S. Moretti, K. Odagiri, *et. al.*, *HERWIG 6: An Event generator for hadron emission reactions with interfering gluons (including supersymmetric processes)*, *JHEP* **0101** (2001) 010, [hep-ph/0011363].

[27] J. Butterworth, J. R. Forshaw, and M. Seymour, *Multiparton interactions in photoproduction at HERA*, *Z. Phys. C* **72** (1996) 637, [hep-ph/9601371].

[28] T. Sjöstrand, S. Mrenna, and P. Z. Skands, *PYTHIA 6.4 Physics and Manual*, *JHEP* **0605** (2006) 026, [hep-ph/0603175].

[29] M. Aliev, H. Lacker, U. Langenfeld, S. Moch, P. Uwer, and M. Widermann, *HATHOR – HAdronic Top and Heavy quarks crOss section calculatoR*, *Comput. Phys. Commun.* **182** (2011) 1034, [arXiv:1007.1327].

[30] N. Kidonakis, *Next-to-next-to-leading-order collinear and soft gluon corrections for t-channel single top quark production*, *Phys. Rev.* **D83** (2011) 091503, [arXiv:1103.2792].

[31] N. Kidonakis, *NNLL resummation for s-channel single top quark production*, *Phys. Rev.* **D81** (2010) 054028, [arXiv:1001.5034].

[32] N. Kidonakis, *Two-loop soft anomalous dimensions for single top quark associated production with a W- or H-*, *Phys. Rev.* **D82** (2010) 054018, [arXiv:1005.4451].

[33] S. Frixione, E. Laenen, P. Motylinski, and B. R. Webber, *Single-top production in MC@NLO*, *JHEP* **0603** (2006) 092, [hep-ph/0512250].

[34] M. L. Mangano, M. Moretti, F. Piccinini, R. Pittau, and A. D. Polosa, *ALPGEN, a generator for hard multiparton processes in hadronic collisions*, *JHEP* **0307** (2003) 001, [hep-ph/0206293].

[35] J. Pumplin, D. Stump, J. Huston, H. Lai, P. M. Nadolsky, *et. al.*, *New Generation of Parton Distributions with Uncertainties from Global QCD Analysis*, *JHEP* **0207** (2002) 012, [hep-ph/0201195].

[36] R. Gavin, Y. Li, F. Petriello, and S. Quackenbush, *W physics at the LHC with FEWZ 2.1*, arXiv:1201.5896.

[37] R. Gavin, Y. Li, F. Petriello, and S. Quackenbush, *FEWZ 2.0: A code for hadronic Z production at next-to-next-to-leading order*, *Comput. Phys. Commun.* **182** (2011) 2388–2403, [arXiv:1011.3540].

[38] J. M. Campbell, R. Ellis, and C. Williams, *Vector boson pair production at the LHC*, *JHEP* **1107** (2011) 018, [arXiv:1105.0020].

[39] Z. Was and P. Golonka, *TAUOLA as tau Monte Carlo for future applications*, *Nucl. Phys. Proc. Suppl.* **144** (2005) 88–94, [hep-ph/0411377].

[40] E. Barberio, B. van Eijk, and Z. Was, *PHOTOS: A universal Monte Carlo for QED radiative corrections in decays*, *Comput. Phys. Commun.* **66** (1991) 115.

[41] **ATLAS** Collaboration, *New ATLAS event generator tunes to 2010 data*, *ATLAS-PHYS-PUB-2011-008*. https://cdsweb.cern.ch/record/1345343.

[42] **ATLAS** Collaboration, *ATLAS tunes of PYTHIA 6 and Pythia 8 for MC11*, *ATL-PHYS-PUB-2011-009*. https://cdsweb.cern.ch/record/1363300.

[43] **GEANT4** Collaboration, S. Agostinelli *et. al.*, *GEANT4: A simulation toolkit*, *Nucl. Instrum. Meth.* **A506** (2003) 250–303.

[44] **ATLAS** Collaboration, *The ATLAS Simulation Infrastructure*, *Eur. Phys. J. C* **70** (2010) 823, [arXiv:1005.4568].

[45] **ATLAS** Collaboration, *Electron performance measurements with the ATLAS detector using the 2010 LHC proton-proton collision data*, *Submitted to Eur. Phys. J. C* (2011) [arXiv:1110.3174].

[46] **ATLAS** Collaboration, *Muon reconstruction efficiency in reprocessed 2010 LHC proton-proton collision data recorded with the ATLAS detector*, *ATLAS-CONF-2011-063*. https://cdsweb.cern.ch/record/1345743.

[47] M. Cacciari, G. P. Salam, and G. Soyez, *The anti-k(t) jet clustering algorithm*, *JHEP* **0804** (2008) 063, [arXiv:0802.1189].

[48] M. Cacciari and G. P. Salam, *Dispelling the N**3 myth for the k(t) jet-finder*, *Phys. Lett. B* **641** (2006) 57, [hep-ph/0512210].

[49] W. Lampl *et. al.*, *Calorimeter Clustering Algorithms: Description and Performance*, *ATL-LARG-PUB-2008-002*. https://cdsweb.cern.ch/record/1099735.

[50] **ATLAS** Collaboration, *Jet energy measurement with the ATLAS detector in proton-proton collisions at* $\sqrt{s} = 7$ *TeV*, arXiv:1112.6426.

[51] **ATLAS** Collaboration, *Validating the measurement of jet energies with the ATLAS detector using Z+jet events from proton-proton collisions at* $\sqrt{s} = 7$ *TeV*, *ATLAS-CONF-2011-159*. https://cdsweb.cern.ch/record/1403179.

[52] **D0** Collaboration, V. Abazov *et. al.*, *Measurement of the* $p\bar{p} \to t\bar{t}$ *production cross section at* $\sqrt{s} = 1.96$ *TeV in the fully hadronic decay channel.*, *Phys. Rev.* **D76** (2007) 072007, [hep-ex/0612040].

[53] **ATLAS** Collaboration, *Commissioning of the ATLAS high-performance b-tagging algorithms in the 7 TeV collision data*, *ATLAS-CONF-2011-102*. http://cdsweb.cern.ch/record/1369219.

[54] **ATLAS** Collaboration, *Performance of the Reconstruction and Identification of Hadronic Tau Decays with ATLAS*, *ATLAS-CONF-2011-152*. http://cdsweb.cern.ch/record/1398195.

[55] **ATLAS** Collaboration, *Performance of Missing Transverse Momentum Reconstruction in Proton-Proton Collisions at* $\sqrt{s} = 7$ *TeV with ATLAS*, *Eur. Phys. J. C* **72** (2012) 1844, [arXiv:1108.5602].

[56] E. Gross and O. Vitells, *Transverse mass observables for charged Higgs boson searches at hadron colliders*, *Phys. Rev.* **D81** (2010) 055010, [arXiv:0907.5367].

[57] **ATLAS** Collaboration, *Search for neutral MSSM Higgs bosons decaying to* tau^+tau^- *pairs in proton-proton collisions at* $\sqrt{s} = 7$ *TeV with the ATLAS detector*, *Phys. Lett.* **B705** (2011) 174–192, [arXiv:1107.5003].

[58] **ATLAS** Collaboration, *ATLAS Muon Momentum Resolution in the First Pass Reconstruction of the 2010 p-p Collision Data at* $\sqrt{s} = 7$ *TeV*, *ATLAS-CONF-2011-046*. http://cdsweb.cern.ch/record/1338575.

[59] S. Frixione, P. Nason, and C. Oleari, *Matching NLO QCD computations with Parton Shower simulations: the POWHEG method*, *JHEP* **11** (2007) 070, [arXiv:0709.2092].

[60] P. Skands, *Tuning Monte Carlo generators: The Perugia tunes*, *Phys. Rev. D* **82** (2010) 074018.

[61] G. Cowan, K. Cranmer, E. Gross, and O. Vitells, *Asymptotic formulae for likelihood-based tests of new physics*, *Eur. Phys. J. C* **71** (2011) 1554, [arXiv:1007.1727].

[62] M. S. Carena, S. Heinemeyer, C. E. M. Wagner, and G. Weiglein, *Suggestions for benchmark scenarios for MSSM Higgs boson searches at hadron colliders*, *Eur. Phys. J. C* **26** (2003) 601–607, [hep-ph/0202167].

[63] A. L. Read, *Presentation of search results: The CL(s) technique*, *J. Phys.* **G28** (2002) 2693–2704.

[64] S. Heinemeyer, W. Hollik, and G. Weiglein, *FeynHiggs: A program for the calculation of the masses of the neutral CP-even Higgs bosons in the MSSM*, *Comput. Phys. Commun.* **124** (2000) 76–89, [hep-ph/9812320].

[65] S. Dittmaier, C. Mariotti, G. Passarino, R. Tanaka, *et. al.*, *Handbook of LHC Higgs Cross Sections: 2. Differential Distributions*, *CERN-2012-002* (2012) [arXiv:1201.3084].

[66] M. Carena, D. Garcia, U. Nierste, and C. E. M. Wagner, *Effective lagrangian for the* $\bar{t}bH^+$ *interaction in the MSSM and charged Higgs phenomenology*, *Nucl. Phys.* **B577** (2000) 88–120, [hep-ph/9912516].